Chemical Engineering Journal Advances 2 (2020) 100017

Contents lists available at ScienceDirect

Chemical Engineering Journal Advances

journal homepage: www.elsevier.com/locate/ceja

Graphene oxide for efficient treatment of real contaminated water by mining tailings: Metal adsorption studies to Paraopeba river and risk assessment

Yuri Abner Rocha Lebron[a], Victor Rezende Moreira[a], Guilherme Pinheiro Drumond[b], Marielle Mara da Silva[b], Rafael de Oliveira Bernardes[b], Lucilaine Valéria de Souza Santos[a,b], Raquel Sampaio Jacob[c], Marcelo Machado Viana[d,*], Cláudia Karina Barbosa de Vasconcelos[b,d,e]

[a] Departamento de Engenharia Sanitária e Ambiental, Universidade Federal de Minas Gerais, Belo Horizonte, MG ZIP 30.270-901, Brazil
[b] Departamento de Engenharia Química, Pontifícia Universidade Católica de Minas Gerais, Belo Horizonte, MG ZIP 30.270-901, Brazil
[c] Departamento de Engenharia Civil, Pontifícia Universidade Católica de Minas Gerais, Belo Horizonte, MG ZIP 30.270-901, Brazil
[d] Departamento de Química, Universidade Federal de Minas Gerais, Belo Horizonte, MG ZIP 30.270-901, Brazil
[e] Departamento de Física e Química, Pontifícia Universidade Católica de Minas Gerais, Belo Horizonte, MG ZIP 30.270-901, Brazil

ARTICLE INFO

Keywords:
Adsorption
Nanotechnology
Graphene oxide
Water treatment

ABSTRACT

The present study aimed at the GO synthesis by a modified Hummers method; and to evaluate the GO's efficiency for heavy metals adsorption in a real surface water sample, collected after a tailing dam rupture in the state of Minas Gerais Brazil. Furthermore, the acute and chronic risks by using a Hazard Quotient (HQ) method was used in order to assess the environmental impact related to raw surface water, and its reduction after GO treatment. The characterization techniques demonstrated that GO had a few-layers (~8 sheets) with micrometric dimensions containing some submicron sized sheets. Furthermore, the BET revealed that the GO had a considerable specific surface area, which favored the adsorption processes. Total dissolved solids and pH met the criteria established by national standards, even after the tailing dam rupture. Conversely, all heavy metal ions presented concentration values greater than recommended. In terms of removal efficiency, higher values were obtained for copper, manganese and aluminum, which were higher than 90.2%. Due to its high concentration in untreated surface water, iron poses a high risk (39.1 mg/L; HQ > 1) in cases of chronical consumption of the contaminated water. After adsorption process, the hazard index value was lower than one, which suggests that population is unlikely to experience adverse health effects. The results reinforce the GO applicability in surface water treatment, even in real and complex aqueous solutions as considered throughout this study.

1. Introduction

On January 25th, 2019, a Dam "B1" of the "Córrego do Feijão" containing mining tailings, in Brumadinho, Minas Gerais - Brazil collapsed, immediately impacting 703 people and the surrounding ecosystem [1]. The rupture caused the death of 259 people and 11 are considered as permanent missing, according to reports found until January 2020. Approximately 12 million cubic meters of iron mining tailings were released from the ruptured reservoir which led to a series of social, environmental and economic impacts covering a vast territory [2,3]. Most of the mining tailings firstly reached the "Córrego do Feijão", which is a tributary of Paraopeba river. The contamination of the Paraopeba river also occurred and, because of that, this river has been constantly monitored by a national institute responsible for water management called IGAM (*Instituto Mineiro de Gestão das Águas*) [4]. According to IGAM, the water quality of this river has been assessed for physical-chemistry characteristics such as turbidity measurements and the presence of dissolved metals. In particular, it was reported that, in the 60 days following the dam rupture (end of January to April), the presence of iron, manganese, aluminum among others in amounts that precluded the use of the river water for the most diverse purposes such as human and animals consumption, irrigation in agriculture, aquaculture and fishing. Nowadays, an oscillation in the quality of the river continues to occur mainly due to rainfalls which contributed to the remobilization of the material deposited in the riverbed and riverbanks.

Vergilio et al. [5] reported that after the dam rupture, an enrichment in metal levels along the Paraopeba river occurred, mainly with Fe, Al, Mn, Zn, Cu, Pb, Cd and U, which were higher than those limits allowed by Brazilian environmental legislation. Thompson et al. [6] showed the

* Corresponding author.
E-mail address: marcelomachado@ufmg.br (M.M. Viana).

https://doi.org/10.1016/j.ceja.2020.100017
Received 30 July 2020; Received in revised form 27 August 2020; Accepted 28 August 2020

changes in the water quality across 464 km of the Paraopeba river in the week after the disaster and during four months later. They reported high turbidity values, in addition to metal and nutrients in elevated levels after the disaster. Moreover, toxicity tests using zebrafish embryo showed high mortality rates even after four months since the accident, because of the deteriorated water quality in the studied area.

The accumulation of metallic ions in the human organism is also extremely prejudicial. As an example, trace metals like lead and cadmium, which cannot be metabolized by humans – therefore bioaccumulate, may cause brain damage, respiratory and kidney malfunctions, and specially, have an impact on the nervous system [7]. So, water contaminated by these metals become an extremely relevant subject. Thus, besides the possibility of aggravating chronic and acute diseases in the region, this water course that supplies the region would have its use compromised. Additionally, when these mining tailings dry, high exposure to a mineral-rich dust could lead to a disturbing allergic condition, affecting primarily the respiratory and cutaneous systems [8].

Many treatment methods have been used to remediate the metal contaminations such as chemical precipitation, ion-exchange, adsorption membrane filtration, co-precipitation/adsorption, electrodialysis, among others [9,10]. Adsorption process is a consolidated technology which overcomes one of the major drawbacks related to the previously mentioned technologies, which is their incapability of retaining the contaminants when a low concentration gradient is involved. A series of adsorbents have been tested in recent years [11–15], and a special attention has been given to nanomaterials as graphene and graphene oxide.

A derivative of graphene, the graphene oxide (GO), has proved particularly useful in several areas due to its relatively easy manufacturing, the presence of different functional groups and its high electronic density [16]. Moreover, GO not only acts as an effective adsorbent but a few studies also accomplished its desorption and regeneration, recovering up to 90% of its adsorption capacity [17]. These characteristics represents advantages to its use as adsorbent if compared to other carbonaceous materials. Even so, advancements in synthesis and characterization of GO are still required to scale-up its application. For instance, depending on oxidation protocol it could demand on the use of strong acids (leading to subsequent environmental issues), longer reaction times and purification processes, which could result in high manufacture costs [18,19].

Sadeghi et al. [20] developed graphene oxide nanoribbons for arsenic and mercury adsorption in aqueous solutions and they confirm the nanomaterial efficiency in the remediation of these elements. Furthermore, another study [21] demonstrated that combined effects of GO-heavy metal ion complexes show different bioavailability and toxicity compared to GO and metal ions separately. In particular, the complex formed after adsorption process presented a significantly reduction in toxicity, an important initial result to assess the ecological risk of carbon nanomaterials. Wang et al. [22] assessed the removal efficiency of several trace metals found in a real effluent by a novel graphene oxide-ordered mesoporous silica material. These authors reported efficiencies higher than 78.7% for several ions such as As, Cd, Cr, Hg, and Pb. Ghorbani et al. [23] showed that a magnetic ethylene diamine-functionalized graphene oxide was able to remove 99.6 and 99.4% of Pb and Cd respectively from a real electroplating wastewater. To the best of our knowledge there is not a paper assessing the efficiency of GO in aquatic systems affected by mining tailings.

From the studies reported, it is noted that the most promising results in terms of adsorption capacity were obtained at ambient temperature and neutral pH as experimental conditions. The fact could be comprehended as an advantage since it would exempt the treatment process from chemical inputs, for a pH adjustment, or high energy demand, for temperature control; therefore, lowering operation expenditures when GO is applied for water treatment. However, a greater limitation in these studies are their assessment of GO efficiency in a synthetic aqueous solution composed of a single metal ion, which does not represent the complexity of real surface water samples. In that case, removal efficiencies may be affected, as well as adsorption capacity since a competition would occur between the different pollutants and the material active sites.

Therefore, the present study intends to synthesize GO by a modified Hummers method; and to evaluate the GO's efficiency for heavy metals remediation in a real surface water sample, collected after a tailing dam rupture in the state of Minas Gerais Brazil. For that, the material was characterized, and batch adsorption tests were conducted. In addition to removal efficiency, the acute and chronic risks estimation by the Hazard Quotient (HQ) method was used in order to assess the environmental impact related to raw surface water, and its reduction after GO treatment.

2. Materials and methods

2.1. Chemicals and reagents

Graphene oxide were prepared with expandable flake graphite (CAS 12,777–87–6) purchased from Asbury Graphite Mills, Inc. Sulfuric acid (H_2SO_4), phosphoric acid (H_3PO_4), potassium permanganate ($KMnO_4$), hydrogen peroxide (H_2O_2) and hydrochloric acid (HCl) were also used, all of them purchased from Sigma-Aldrich (St. Louis, MO, USA).

2.2. Graphene oxide preparation

The first step involved the preparation of expanded graphite (EG) from graphite in a furnace at 800 °C for 30 min. The EG was then used to prepare graphene oxide (GO) using the modified Hummers method [24]. 50 mg of EG was added to a solution of phosphoric acid and sulfuric acid 1:9 in volume, respectively. Then, potassium permanganate ($KMnO_4$) was slowly added to the mixture in the EG:$KMnO_4$ (1:5 mass ratio) which remained under agitation at 50 °C for 1 h. After, 50 mL of deionized water was added to the dispersion, which was sonicated for 2 h. To reduce the manganese oxides formed to manganese ions, hydrogen peroxide (30%vol.) was added to the system. After washing with water and subsequent centrifugation (pH~6), the material obtained was freeze-dried to obtain GO powder.

2.3. Graphene oxide characterization

The GO morphology and structure was assessed by a TEM microscope (FEI Tecnai G2–20) operating at 200 kV and the corresponding selected area electron diffraction (SAED) pattern. The GO powder was deposited on a copper grid Holey Carbon (300 mesh). The GO structure was investigated by X-ray diffraction (XRD), on a Rigaku D/Max 2550, using copper Kα radiation (λ = 1.5418 Å) set to 40 kV at 30 mA. XRD patterns were collected at a scanning rate of 2° min^{-1}. The average number of graphene sheets was determined by using the Debye-Scherrer equation (Eq. (1)) [25]:

$$t = \frac{0.89\ \lambda}{\beta_{002} \cos\theta_{002}} \quad (1)$$

$$n = \frac{t}{d_{002}} \quad (2)$$

where t is the thickness of layers, β is the full width at half maxima (FWHM), n (Eq. (2)) is the number of layers, d is the interlayer spacing and θ is the diffraction angle.

The chemical composition of graphene oxide was analyzed by X-ray photoelectron spectroscopy (XPS), using a K_α X-ray photoelectron spectrometer (Thermo Fisher Scientific) equipped with hemispherical electron analyzer and monochromatic Al K_α (1486.6 eV) radiation. The incident radiation diameter was maintained at 400 μm throughout the experiment. Survey scans were performed using a 200 eV pass energy, The data were analyzed and the peak deconvolution was performed using the Thermo Avantage Software.

Thermogravimetric analysis (TGA) was carried out using a Shimadzu Thermal Analyzer (DTG-60H) at a heating rate of 10 °C/min from room

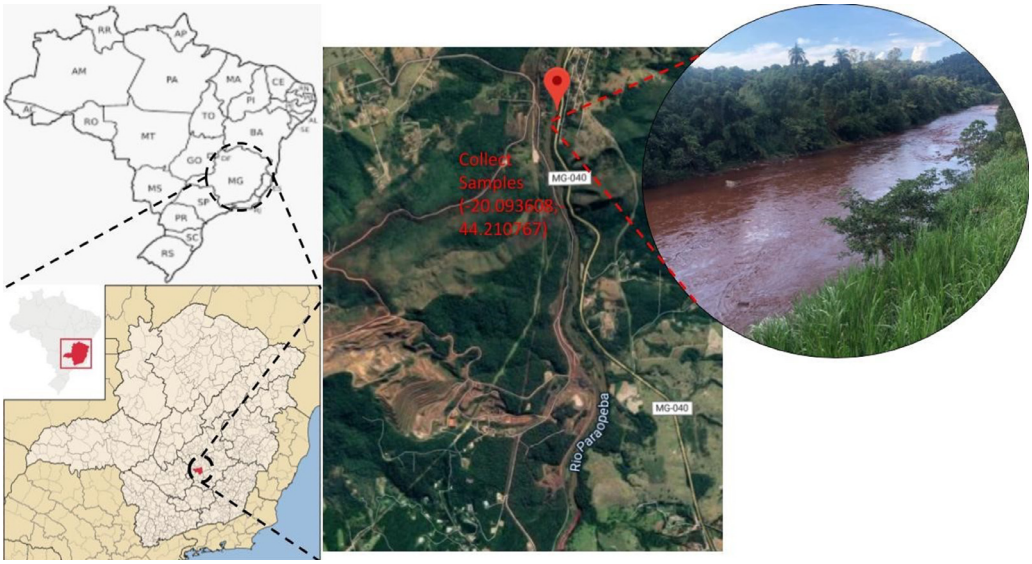

Fig. 1. Sample collection site in the metropolitan region of a Brazilian city (Belo Horizonte, Minas Gerais, −20.093608, −44.210767), after a mining tailing dam rupture.

temperature (~28 °C) to 900 °C. All the experiments were performed under nitrogen atmosphere at a flow rate of 50 mL/min. GO was also structurally characterized by Raman spectroscopy (950 cm^{-1} to 3000 cm^{-1}) using a Senterra from Bruker, coupled with an OLYMPUS BX51 optical microscope, 532 nm laser and 10 mW power. Specific surface area and porosity were evaluated by N_2 gas adsorption technique (QuantaChrome/NOVA 1200e), employing BET and BJH methods, respectively.

2.4. Sample site and adsorption tests

The surface water sample was collected after a mining tailing dam rupture, which the site is represented in Fig. 1.

Water samples were collected 18.6 km from the dam rupture site, following the methodology suggested by the US Environmental Protection Agency (EPA-US) [26], and were characterized according to the *Standard Methods for the Examination of Water and Wastewater* [27]. Along the affected area, the water was found under degraded conditions, and the government's recommendation was that untreated water should not be used for human consumption, nor for animal consumption or agricultural purposes.

Except for mercury and total arsenic, all other ions were determined in house using an atomic absorption spectrophotometer (Shimadzu, AA-7000) and an external calibration curve (R^2>0.99 for all ions). Mercury and total arsenic ions were determined by an external lab using the standard methods 3112B, 3030B and 3114B All measurements were performed in triplicate.

The adsorption experiments were conducted in media containing 10 mL of the surface water with a graphene oxide concentration of 200 mg/L. The system was kept under constant agitation (250 rpm) and room temperature in an orbital shaker (Marconi MA420) for 24 h. Aliquots were then collected and centrifuged at 4000 rpm (Excelsa® 2260, Fanem), and the supernatant used to determine the physicochemical parameters after the treatment proposed.

The experiment was performed in triplicate and its efficiency was evaluated in terms of the pollutant removal efficiency (%), calculated by Eq. (3).

$$Removal = 100 \cdot \left(C_0 - C_e\right)/C_0 \tag{3}$$

Where C_0 (mg•L^{-1}) and C_e (mg•L^{-1}) are the initial and equilibrium concentration, respectively.

2.5. Risk assessment

The toxicity posed by the heavy metals was assessed considering the chronic effects over a prolonged exposure, prior and after the treatment process proposed. For that the non-carcinogenic risk commonly characterized by a hazard quotient (HQ; Eq. (4)) was considered, which considers the chronic daily intake and a given compound reference dose (*RfD*). For a single constituent, the chronic daily intake (*CDI*) is obtained by Eq. (5), in which *C* corresponds to the metal ion concentration, *DI* to the water consumption in a daily intake basis (2 L) and *BW* to the average body weight from the local community (70 kg). Complementarily, the hazard index (*HI*) was also determined to assess the risk posed from all different species, which can be obtained through Eq. (6).

$$HQ = \frac{CDI}{RfD} \tag{4}$$

$$CDI = \frac{C \cdot DI}{BW} \tag{5}$$

$$HI = \sum HQ_i = \sum \frac{CDI_i}{RfD_i} \tag{6}$$

3. Results and discussion

3.1. Graphene oxide characterization

Fig. 2(a) shows the presence of few-layers GO structure with micrometric dimensions containing some submicron sized GO sheets probably formed during the sonication process.

The crystallographic structure of the graphene oxide sheets was characterized by SAED technique (Fig. 2(b)). Most of the sheets exhibited a single set of hexagonal diffraction (the 6-fold pattern is consistent with a hexagonal lattice) and spots relatively well defined associated to AB Bernal-stacked graphite [28]. Moreover, the small elongation observed for the spots indicates that the domains have few rotational stacking faults. The basal plane in graphene-like structures are subject to stacking faults and accommodates basal dislocations/twists [29]. In particular, the SAED pattern shown here evidenced that few rotational stacking faults between GO layers are present. The absence of multiple spots in SAED pattern and the inner hexagon with 0.21 nm spacing confirms the presence of a crystalline structure with almost no crystal defect [30].

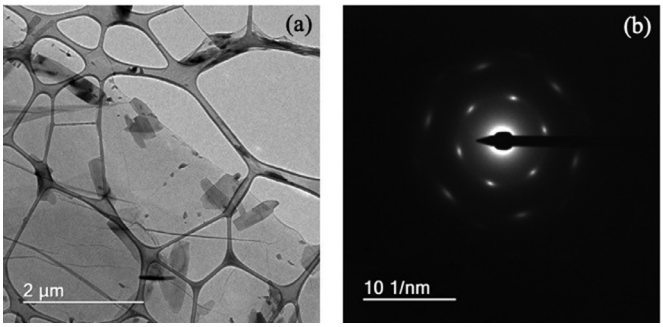

Fig. 2. (a) TEM image and (b) SAED pattern of the graphene oxide prepared.

Table 1
Elemental percentage obtained from C1s and O1s XPS survey spectra of GO.

	Binding Energy (eV)	Atomic%
C1s	286.90	66.7
O1s	533.14	33.3

Fig. 3(a) shows the XRD patterns of graphite and graphene oxide. The (0 0 2) crystal plane of graphite was evident as intense crystalline peak was found at $2\theta = 26.6^{\circ}$ (lattice spacing of 0.34 nm) [31]. This peak shifts to $2\theta = 10.7^{\circ}$ (interplanar distance of 0.81 nm) indicating the success in oxidation in GO preparation. The FWHM allowed to estimate the average number of layers (n) to GO and the values found were 8 sheets. The intercalation with water and the presence of oxygen functionalities on the basal plane of the carbon sheet result in an increase in interlayer spacing [32–35].

The XPS survey spectrum (Fig. 3(b)) confirmed the presence of C and O signals. The surface compositions determined from this spectrum are presented in Table 1.

Fig. 4 presents the thermogravimetry curves (TG) in black and derivative thermogravimetry (DTG) in blue for graphite and GO.

The graphite curves (Fig. 4(a)) shows a significant weight loss at 675 °C due to combustion. In contrast, the GO curves showed a three-step weight loss in the temperature range analyzed. The initial weight loss (22%) started below 100 °C and was attributed to loss of water molecules. The second event is observed in a temperature range from 160 °C to 270 °C and the mass loss (33%) is assigned to the removal of oxygen containing functional groups [31]. These results are in accordance with the XPS analysis presented by Fig. 3(b) and Table 1, that indicates a 33.3% of oxygen atomic percentage. Finally, the major mass (45%) loss occurs between 360 °C and 550 °C which is attributed to the combustion of the basal carbon structure [36,37].

The Raman spectra (Fig. 5(a)) exhibit two main characteristic bands of graphite structures, the G band (E_{2g} mode) at ~1575 cm^{-1} associated to sp^2 carbon vibration and the D band (defect induced mode) at ~1350 cm^{-1} related to disordered structure of graphene [38]. The 2D band at ~2700 cm^{-1} and $D + D$" band at ~ 2450 cm^{-1} showed by expanded graphite are originate from D phonons and an acoustic longitudinal phonon (D") and are associated to electronic band structure and number of graphene layers [39]. These set of bands at the range 2300 cm^{-1} to 2800 cm^{-1} observed for EG sample vanished for the GO sample. In particular, the G band broadens considerably for GO sample, and it is blue-shifted ($\Delta\nu = 12$ cm^{-1}) when compared to that for EG sample. Indeed, the increase of the structural defects in graphite due to oxidation and exfoliation processes causes the appearance of a D' band (a defect mode) at ~ 1620 cm^{-1}, which partially merges with the G band in GO sample [40–42]. The determination of I_D/I_G ratio has been used to verify the induced structural disorder. The I_D/I_G ratio changed from 0.03 (EG) to 0.97 (GO) confirming the decrease in the size of sp^2 domains upon chemical exfoliation. However, the G band still maintain its highest intensity ($I_D/I_G < 1$), which demonstrate that the GO sheets prepared has a low defect content [43]. This result is corroborated by TEM image and SAED pattern previously presented and discussed here.

Fig. 5(b) shows the N_2 isotherm and pore size distribution of as-prepared graphene oxide. The specific surface area (SSA) is about 67 $m^2 g^{-1}$. The C constant value of 38 ($0.05<P/Po<0.3$) and the linear coefficient correlation (r) above 0.999 confirm the reliability of this measurement [44]. The SSA determined suggest that the GO nanosheets prepared show a high degree of layer ordering maintaining low structural distortion due to sp^3 carbon presence and also indicates the occurrence of a preferential oxidation process at the sheet edges [45]. The isotherm shows a hysteresis type H3 resulted from slit-shaped pores between parallel layers, characteristic of graphene related materials [46]. The bimodal pore size distribution observed (micro and mesopores) expands the potential of graphene oxide applications in adsorptive processes.

3.2. GO as an adsorbent

The main physicochemical properties for the surface water before and after its treatment is presented in Table 2. For comparison purposes, the Brazilian national standard limits were also included, stablishing threshold values for surface water designated for human consumption after conventional water treatment (coagulation-flocculation, followed by disinfection and a pH correction whenever necessary) and leisure in which a primary contact occurs.

Among the physicochemical properties, pH and total dissolved solids (TDS) attains the national standards regardless of the tailing dam rupture. Generally, TDS are retained by the filters in drinking water treatment plants but, when in high concentrations in raw surface water, may impact the local fauna and flora as it hampers the light assessment required by submerges vegetation; therefore, their biological activity. After adsorption, the pH decreased to values bellow recommended by national standards. The results would be expected considering that graphene oxide present acid functional groups which deprotonated in water, reducing the pH value [47]. Additionally, ion exchange reactions between the metallic species and the proton on carboxyl and hydroxyl

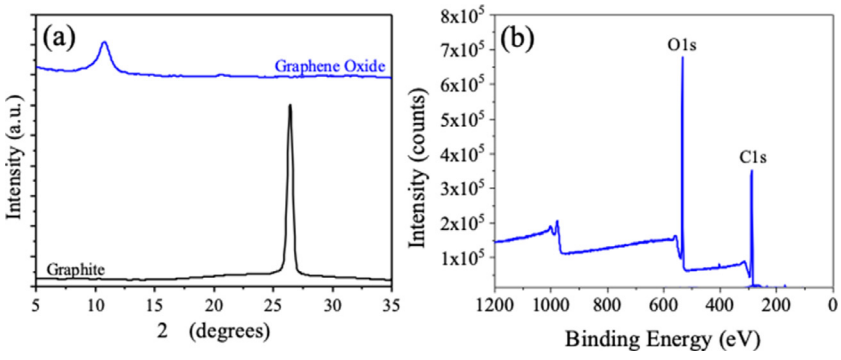

Fig. 3. (a) X-ray diffractograms for graphene oxide (GO) and graphite. (b) XPS survey spectrum of GO.

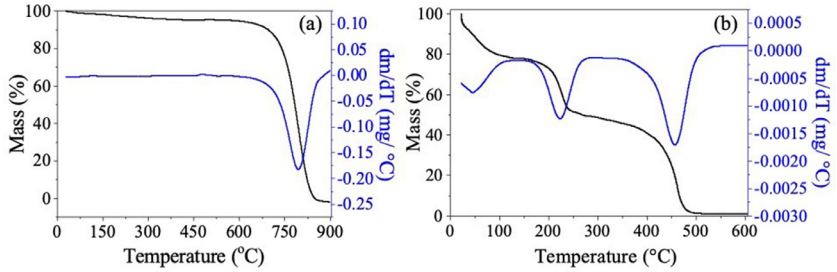

Fig. 4. TGA/DTG curves for (a) expanded graphite and (b) graphene oxide.

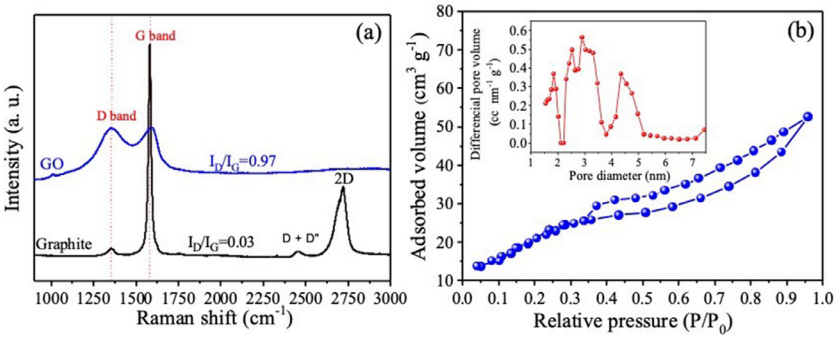

Fig. 5. (a) Raman spectra of as-prepared GO compared with that of expanded graphite (EG). (b) Nitrogen adsorption-desorption isotherms and pore size distribution plot (inset) of GO sample.

Table 2
Paraobepa river and treated water physicochemical properties and GO removal efficiencies. [a] Total dissolved solids.

Parameter	Surface water	Treated water	National standards (CONAMA 357)	Removal (%)
pH	6.59 ± 0.06	5.74 ± 0.02	6.0 – 9.0	–
Conductivity (μS/cm)	247 ± 10	95.18 ± 3.15	–	61.5 ± 2.3
TDS[a] (mg/L)	126.6 ± 0.1	46.50 ± 3.54	< 500	63.3 ± 2.0
Turbidity (NTU)	3350 ± 113	3212 ± 97	< 100	–
Cu (II) (mg/L)	1.23 ± 0.11	< 0.10	< 0.009	> 91.9 ± 0.7
Fe (II) (mg/L)	39.10 ± 2.16	0.50 ± 0.09	< 0.3	98.7 ± 0.2
Mg (II) (mg/L)	1.26 ± 0.09	0.94 ± 0.12	–	22.6 ± 2.4
Mn (II) (mg/L)	8.64 ± 0.20	< 0.10	< 0.1	> 98.8 ± 0.7
Ca (II) (mg/L)	1.38 ± 0.07	0.81 ± 0.06	–	42.2 ± 3.1
Ni (II) (mg/L)	0.27 ± 0.03	< 0.10	< 0.025	> 62.7 ± 1.3
Al (III) (mg/L)	1.02 ± 0.01	< 0.10	< 0.1	> 90.2 ± 0.5
As_{Total} (mg/L)	<0.01	<0.01	< 0.01	–
Hg (II) (mg/L)	<0.0002	<0.0002	< 0.0002	–

functional groups may occur, considering this event as one of the main mechanisms responsible for metallic species sequestration in adsorption process involving GO. For exemplification purposes, the reactions involved were presented in Eqs. (7)–(11) considering copper as a pollutant [48].

$$-COOH + Cu^{2+} \rightarrow -COOCu^{+} + H^{+} \quad (7)$$

$$-OH + Cu^{2+} \rightarrow -OCu^{+} + H^{+} \quad (8)$$

$$-2COOH + Cu^{2+} \rightarrow -COOCuOOC + 2H^{+} \quad (9)$$

$$-2OH + Cu^{2+} \rightarrow -OCuO + 2H^{+} \quad (10)$$

$$-COOH + Cu^{2+} + -OH \rightarrow -COOCuO + H^{+} \quad (11)$$

Despite of pH and TDS, all other parameters were above the national standards in raw surface water sample, which includes all heavy metals. However, after adsorption, manganese and aluminum attained the concentrations limits. Aluminum is considered a highly biologically reactive and essentially toxic, which its chronic consumption is related to Alzheimer's disease, breast cancer and autism [49]. We reinforce that conventional drinking water facilities employ other treatments prior to a tertiary treatment, as the one being proposed in the current study, which also have their contribution to heavy metals removal and the attainment of the threshold stablished in national standards.

The presence of different oxygen-containing functional groups such as -COOH, -C=O, and -OH, in addition to the high material dispersibility in water, favors its application to trace metals remediation in surface water. In addition to the previously mentioned ion exchange mechanism, stable complex formations based on Lewis acid-base interactions would be responsible for the metallic species uptake process, in which graphene oxide acts as a Lewis base, capable of donating electrons, while the metal ion would exhibit an inverse behavior characterized as Lewis acid [17]. Moreover, due to its constitution, the material still has advantages over other carbonaceous adsorbents such as carbon nanotubes, in which would be required an additional oxidation process in order to introduce hydrophilic groups onto its surface aiming at increasing its adsorption capacity. Similar results were observed by [16] while evaluating graphene oxide nanosheets capacity to adsorb cadmium and cobalt from aqueous monometallic solutions. Other property that highlight the GO application for adsorption it is the specific surface area (67 $m^2\ g^{-1}$) which was higher than other studies that synthesized GO by the same methodology. For example, Bele et al. [50] reported a GO with a specific surface area of 20.93 $m^2\ g^{-1}$ and Li et al. [51] 32 $m^2\ g^{-1}$.

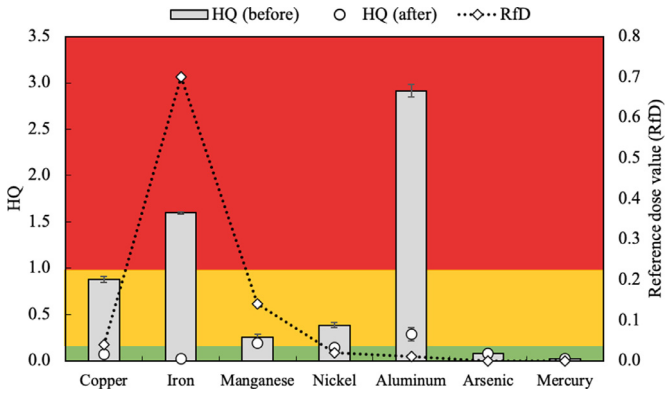

Fig. 6. Hazard quotient indexes before and after the water treatment process.

The reduction on turbidity was not expected, since GO does not have a strong charge neutralization effect as compared to other coagulants such as PAC [52]. Although, the slight reduction on turbidity may be attributed to the sweeping effect. Yang et al. [52] have shown that at neutral or alkaline conditions GO has no significant removal efficiency because charge repulsion between particles is dominant.

Previous studies have shown the GO effectiveness to adsorb different metal ions, but to the best of our knowledge, there is not reports on simultaneous adsorption on real surface water. Gopalakrishnan et al. [53] assessed the GO potential to simultaneously adsorb Pb(II), Ni(II) and Cr(VI). In his study GO (700 mg/L) was able to effectively remove all metal ions on the effluent. Furthermore, Zhang et al. [54] proposed different solvents for bisphenol A desorption from reduced graphene oxide combined with magnetic nanoparticles. In this reference, desorption efficiency varied from approximately 40 to 98%, when cyclohexane and methanol was used, respectively, reporting an effective reusability until the fifth cycle.

3.3. Risk assessment

The results obtained in terms of chronic risks are presented in Fig. 6. HQ values greater than 1 implies in a high risk, whereas HQ values between 0.1 and 1 comprehend medium risks. Finally, HQ values < 0.1 implies in low or negligible risks. In terms of RfD, the greater the value is, lower is the risk posed to human health.

Although iron presented a high RfD, its high concentration in raw surface water imposed a high risk in cases of chronic water consumption. Aluminum, on its turn, was quantified in lower concentration levels; however, due to its high toxicity, HQ values greater than one were also observed for the untreated water sample. When all heavy metal ions were considered, HI values were greater than one (HI_{before} = 6.03) which reassures that water consumption would imposes risks over human health.

After adsorption process, HQ values were lower than 0.1 which indicates low or negligible risks excepting for aluminum. The process was still efficient in terms of copper, magnesium, and nickel toxicity reduction, which initially imposed a medium risk, but were considered to pose a lower or negligible after GO adsorption. As a result, the hazard index value after adsorption process was lower than one (HI_{after} = 0.71) and reinforces the GO effectiveness in a real surface water treatment.

4. Conclusions

Graphene oxide (GO) has proven to be an effective adsorbent for surface water treatment under harsh conditions as experienced in Paraopeba River. Comparing to the national surface water standards, only pH and total dissolved solids were within the limits for the untreated surface water, and all other parameters including heavy metals presented values above the standard limits. The characterization demonstrated that graphite was converted to GO, which showed a structure of few-layers with micrometric dimensions containing some submicron sized sheets. The XPS survey spectra showed a significant content of oxygen, which may be attributed to oxygenated functional groups. Furthermore, the BET revealed that the GO had a considerable specific superficial area, which favored the adsorption processes. Graphene oxide efficiency in heavy metals sequestration was later proven in a batch adsorption process. Among all metals, aluminum, copper and manganese presented removal rates greater than 90.2%. Despite of that, aluminum would still pose a medium risk over chronic water consumption. The results obtained reinforces GO capability in heavy metals sequestration, and its efficiency was reassured even in a complex medium.

Declaration of Competing Interest

The authors declare that they have no known competing financial interests or personal relationships that could have appeared to influence the work reported in this paper.

Acknowledgments

The authors would like to thank Fundação de Amparo à Pesquisa de Minas Gerais (Fapemig), Conselho Nacional de Desenvolvimento Científico e Tecnológico (CNPq) and Coordenação de Aperfeiçoamento de Pessoal de Nível Superior – Brasil (CAPES) – Finance Code 001 for the financial support received. The authors would like to acknowledge the Center of Microscopy at the Universidade Federal de Minas Gerais (http://www.microscopia.ufmg.br) for providing the equipment and technical support for experiments involving electron microscopy and the Nanotechnology Laboratory (LNNano) by XPS measurements (Proposals XPS-24609 and XPS-24668).

References

[1] D.da S. Noal, I.V.M. Rabelo, E. Chachamovich, The mental health impact on individuals affected by the vale dam rupture, Cad. Saude Publica. 35 (2019) 1–7 https://doi.org/10.1590/0102-311X00048419.
[2] J.L. Porsani, F.A.N. de Jesus, M.C. Stangari, GPR survey on an iron mining area after the collapse of the tailings Dam I at the Córrego do Feijão mine in Brumadinho-MG, Brazil, Remote Sens. 11 (2019) 860–873 https://doi.org/10.3390/RS11070860.
[3] L.H. Silva Rotta, E. Alcântara, E. Park, R.G. Negri, Y.N. Lin, N. Bernardo, T.S.G. Mendes, C.R. Souza Filho, The 2019 Brumadinho tailings dam collapse: possible cause and impacts of the worst human and environmental disaster in Brazil, Int. J. Appl. Earth Obs. Geoinf. 90 (2020) 1–12 https://doi.org/10.1016/j.jag.2020.102119.
[4] I.M. de G. das Águas, Avaliação da qualidade da água e sedimentos do Rio Paraopeba - Acompanhamento da Qualidade das Águas do Rio Paraopeba Após 1 ano do Rompimento da Barragem da Mina Córrego Feijão da Mineradora Vale/SA – Brumadinho/MG, Belo Horizonte, 2020.
[5] C.dos S. Vergilio, D. Lacerda, B.C.V. de Oliveira, E. Sartori, G.M. Campos, A.L. de, S. Pereira, D.B. de Aguiar, T.da S. Souza, M.G. de Almeida, F. Thompson, C.E. de Rezende, Metal concentrations and biological effects from one of the largest mining disasters in the world (Brumadinho, Minas Gerais, Brazil), Sci. Rep. 10 (2020) 1–12 https://doi.org/10.1038/s41598-020-62700-w.
[6] F. Thompson, B.C. de Oliveira, M.C. Cordeiro, B.P. Masi, T.P. Rangel, P. Paz, T. Freitas, G. Lopes, B.S. Silva, A.S. Cabral, M. Soares, D. Lacerda, C.dos Santos Vergilio, M. Lopes-Ferreira, C. Lima, C. Thompson, C.E. de Rezende, Severe impacts of the Brumadinho dam failure (Minas Gerais, Brazil) on the water quality of the Paraopeba River, Sci. Total Environ. 705 (2020) 135914 https://doi.org/10.1016/j.scitotenv.2019.135914.
[7] M.E. Mahmoud, M.M. Osman, A.A. Yakout, A.M. Abdelfattah, Water and soil decontamination of toxic heavy metals using aminosilica-functionalized-ionic liquid nanocomposite, J. Mol. Liq. 266 (2018) 834–845 https://doi.org/10.1016/j.molliq.2018.06.055.
[8] A. Romão, C. Froes, C. Barcellos, D.X. Silva, R. Saldanha, R. Gracie, V. Pascoal, Avaliação preliminar dos impactos sobre a saúde do desastre da mineração da Vale (Brumadinho, MG), in: desastr, Da Val. Em Brum. – Impactos Sobre a Saúde e Desafios Para a Gestão Riscos 1 (2019) 1–12.
[9] F. Fu, Q. Wang, Removal of heavy metal ions from wastewaters: a review, J. Environ. Manage 92 (2011) 407–418 https://doi.org/10.1016/j.jenvman.2010.11.011.
[10] M. Ince, O.K. Ince, Heavy metal removal techniques using response surface methodology: water/wastewater treatment, Toxic. Nanomater., IntechOpen (2019).
[11] M. V.R., L. Y.A.R., L.C. Lange, S. L.V.S., Simultaneous biosorption of Cd(II), Ni(II) and Pb(II) onto a brown macroalgae Fucus vesiculosus: mono- and multi-component isotherms, kinetics and thermodynamics, J. Environ. Manage. 251 (2019) 109587 https://doi.org/10.1016/j.jenvman.2019.109587.

[12] V.R. Moreira, Y.A.R. Lebron, S.J. Freire, L.V.S. Santos, F. Palladino, R.S. Jacob, Biosorption of copper ions from aqueous solution using Chlorella pyrenoidosa: optimization, equilibrium and kinetics studies, Microchem. J 145 (2019) 119–129 https://doi.org/10.1016/j.microc.2018.10.027.
[13] S.T. Yang, Y. Chang, H. Wang, G. Liu, S. Chen, Y. Wang, Y. Liu, A. Cao, Folding/aggregation of graphene oxide and its application in Cu2 + removal, J. Colloid Interface Sci. 351 (2010) 122–127 https://doi.org/10.1016/j.jcis.2010.07.042.
[14] J. Xu, Z. Cao, Y. Zhang, Z. Yuan, Z. Lou, X. Xu, X. Wang, A review of functionalized carbon nanotubes and graphene for heavy metal adsorption from water: preparation, application, and mechanism, Chemosphere 195 (2018) 351–364 https://doi.org/10.1016/j.chemosphere.2017.12.061.
[15] S.Z.N. Ahmad, W.N.W. Salleh, A.F. Ismail, N. Yusof, M.Z.M. Yusop, F. Aziz, Adsorptive removal of heavy metal ions using graphene-based nanomaterials: toxicity, roles of functional groups and mechanisms, Chemosphere (2020) 126008.
[16] G. Zhao, J. Li, X. Ren, C. Chen, X. Wang, Few-layered graphene oxide nanosheets as superior sorbents for heavy metal ion pollution management, Environ. Sci. Technol. 45 (2011) 10454–10462 https://doi.org/10.1021/es203439v.
[17] W. Peng, H. Li, Y. Liu, S. Song, A review on heavy metal ions adsorption from water by graphene oxide and its composites, J. Mol. Liq. 230 (2017) 496–504 https://doi.org/10.1016/j.molliq.2017.01.064.
[18] J. Chen, B. Yao, C. Li, G. Shi, An improved Hummers method for eco-friendly synthesis of graphene oxide, Carbon N.Y. 64 (2013) 225–229 https://doi.org/10.1016/j.carbon.2013.07.055.
[19] A. Romero, M.P. Lavin-Lopez, L. Sanchez-Silva, J.L. Valverde, A. Paton-Carrero, Comparative study of different scalable routes to synthesize graphene oxide and reduced graphene oxide, Mater. Chem. Phys. 203 (2018) 284–292 https://doi.org/10.1016/j.matchemphys.2017.10.013.
[20] M.H. Sadeghi, M.A. Tofighy, T. Mohammadi, One-dimensional graphene for efficient aqueous heavy metal adsorption: rapid removal of arsenic and mercury ions by graphene oxide nanoribbons (GONRs), Chemosphere 253 (2020) 126647 https://doi.org/10.1016/j.chemosphere.2020.126647.
[21] Y. Gao, X. Ren, J. Wu, T. Hayat, A. Alsaedi, C. Cheng, C. Chen, Graphene oxide interactions with co-existing heavy metal cations: adsorption, colloidal properties and joint toxicity, Environ. Sci. Nano 5 (2018) 362–371 https://doi.org/10.1039/c7en01012e.
[22] X. Wang, Y. Pei, M. Lu, X. Lu, X. Du, Highly efficient adsorption of heavy metals from wastewaters by graphene oxide-ordered mesoporous silica materials, J. Mater. Sci. 50 (2015) 2113–2121 https://doi.org/10.1007/s10853-014-8773-3.
[23] M. Ghorbani, A. Shams, O. Seyedin, N. Afshar Lahoori, Magnetic ethylene diamine-functionalized graphene oxide as novel sorbent for removal of lead and cadmium ions from wastewater samples, Environ. Sci. Pollut. Res. 25 (2018) 5655–5667 https://doi.org/10.1007/s11356-017-0929-7.
[24] W.S. Hummers, R.E. Offeman, Preparation of graphitic oxide, J. Am. Chem. Soc. 80 (1958) 1339 –1339 https://doi.org/10.1021/ja01539a017 .
[25] M. Bera, P.G. Chandravati, P.K. Maji, Facile one-pot synthesis of graphene oxide by sonication assisted mechanochemical approach and its surface chemistry, J. Nanosci. Nanotechnol. 18 (2018) 902–912 https://doi.org/10.1166/jnn.2018.14306.
[26] USEPASurface Water Sampling, 2016 Athens, Georgia https://www.epa.gov/quality/surface-water-sampling .
[27] American Public Health Association (APHA), Standard Methods for the Examination of Water and Wastewater (22 ed), Washington (2019). https://www.mendeley.com/catalogue/db6cdbdb-44da-3890-b585-44cbad3c8b29/.
[28] A.W. Robertson, J.H. Warner, Hexagonal single crystal domains of few-layer graphene on copper foils, Nano Lett 11 (2011) 1182–1189 https://doi.org/10.1021/nl104142k.
[29] R.H. Telling, M.I. Heggie, Stacking fault and dislocation glide on the basal plane of graphite, Philos. Mag. Lett. 83 (2003) 411–421 https://doi.org/10.1080/0950083031000137839.
[30] J.H. Warner, M.H. Rümmeli, T. Gemming, B. Büchner, G.A.D. Briggs, Direct imaging of rotational stacking faults in few layer graphene, Nano Lett 9 (2009) 102–106 https://doi.org/10.1021/nl8025949.
[31] M.M. Viana, M.C.F.S. Lima, J.C. Forsythe, V.S. Gangoli, M. Cho, Y. Cheng, G.G. Silva, M.S. Wong, V. Caliman, Facile graphene oxide preparation by microwave-assisted acid method, J. Braz. Chem. Soc. 26 (2015) 978–984 https://doi.org/10.5935/0103-5053.20150061.
[32] K. Krishnamoorthy, M. Veerapandian, K. Yun, S.J. Kim, The chemical and structural analysis of graphene oxide with different degrees of oxidation, Carbon N. Y 53 (2013) 38–49 https://doi.org/10.1016/j.carbon.2012.10.013.
[33] H. He, T. Riedl, A. Lerf, J. Klinowski, Solid-state NMR studies of the structure of graphite oxide, J. Phys. Chem 100 (1996) 19954–19958 https://doi.org/10.1021/jp961563t.
[34] A. Lerf, H. He, M. Forster, J. Klinowski, Structure of graphite oxide revisited, J. Phys. Chem. B 102 (1998) 4477–4482 https://doi.org/10.1021/jp9731821.
[35] H.H. Huang, K.K.H. De Silva, G.R.A. Kumara, M. Yoshimura, Structural evolution of hydrothermally derived reduced graphene oxide, Sci. Rep. 8 (2018) 1–9 https://doi.org/10.1038/s41598-018-25194-1.
[36] P. Nagaraju, A. Alsalme, A. Alswieleh, R. Jayavel, Facile in-situ microwave irradiation synthesis of TiO2/graphene nanocomposite for high-performance supercapacitor applications, J. Electroanal. Chem. 808 (2018) 90–100 https://doi.org/10.1016/j.jelechem.2017.11.068.
[37] A. Morais, J.P.C. Alves, F.A.S. Lima, M. Lira-Cantu, A.F. Nogueira, Enhanced photovoltaic performance of inverted hybrid bulk-heterojunction solar cells using TiO 2 /reduced graphene oxide films as electron transport layers, J. Photonics Energy 5 (2015) 057408 https://doi.org/10.1117/1.jpe.5.057408.
[38] M.A. Pimenta, G. Dresselhaus, M.S. Dresselhaus, L.G. Cançado, A. Jorio, R. Saito, Studying disorder in graphite-based systems by Raman spectroscopy, Phys. Chem. Chem. Phys. 9 (2007) 1276–1290 https://doi.org/10.1039/b613962k.
[39] S. Roscher, R. Hoffmann, O. Ambacher, Determination of the graphene-graphite ratio of graphene powder by Raman 2D band symmetry analysis, Anal. Methods 11 (2019) 1224–1228 https://doi.org/10.1039/c8ay02619j.
[40] R.J. Nemanich, S.A. Solin, First- and second-order Raman scattering from finite-size crystals of graphite, Phys. Rev. B 20 (1979) 392–401 https://doi.org/10.1103/PhysRevB.20.392.
[41] T. Livneh, T.L. Haslett, M. Moskovits, Distinguishing disorder-induced bands from allowed raman bands in graphite, Phys. Rev. B - Condens. Matter Mater. Phys. 66 (2002) 1–11 https://doi.org/10.1103/PhysRevB.66.195110.
[42] L.G. Cançado, M.A. Pimenta, B.R.A. Neves, M.S.S. Dantas, A. Jorio, Influence of the atomic structure on the Raman spectra of graphite edges, Phys. Rev. Lett. 93 (2004) 1–4 https://doi.org/10.1103/PhysRevLett.93.247401.
[43] G. Wang, B. Wang, J. Park, Y. Wang, B. Sun, J. Yao, Highly efficient and large-scale synthesis of graphene by electrolytic exfoliation, Carbon N. Y 47 (2009) 3242–3246 https://doi.org/10.1016/j.carbon.2009.07.040.
[44] M. Thommes, K. Kaneko, A.V. Neimark, J.P. Olivier, F. Rodriguez-Reinoso, J. Rouquerol, K.S.W. Sing, Physisorption of gases, with special reference to the evaluation of surface area and pore size distribution (IUPAC Technical Report), Pure Appl. Chem. 87 (2015) 1051–1069 https://doi.org/10.1515/pac-2014-1117.
[45] B. Gurzęda, T. Buchwald, M. Nocuń, A. Bąkowicz, P. Krawczyk, Graphene material preparation through thermal treatment of graphite oxide electrochemically synthesized in aqueous sulfuric acid, RSC Adv 7 (2017) 19904–19911 https://doi.org/10.1039/c7ra01678f.
[46] S.J. Gregg, K.S.W. Sing, H.W. Salzberg, Adsorption Surface Area and Porosity, J. Electrochem. Soc. 114 (1967) 279 https://doi.org/10.1149/1.2426447.
[47] C.-.J. Shih, S. Lin, R. Sharma, M.S. Strano, D. Blankschtein, Understanding the pH-dependent behavior of graphene oxide aqueous solutions: a comparative experimental and molecular dynamics simulation study, Langmuir 28 (2012) 235–241 https://doi.org/10.1021/la203607w.
[48] W. Peng, H. Li, Y. Liu, S. Song, Comparison of Pb(II) adsorption onto graphene oxide prepared from natural graphites: diagramming the Pb(II) adsorption sites, Appl. Surf. Sci. 364 (2016) 620–627 https://doi.org/10.1016/j.apsusc.2015.12.208.
[49] C. Exley, The toxicity of aluminium in humans, Morphologie 100 (2016) 51–55 https://doi.org/10.1016/j.morpho.2015.12.003.
[50] S. Bele, V. Samanidou, E. Deliyanni, Effect of the reduction degree of graphene oxide on the adsorption of Bisphenol A, Chem. Eng. Res. Des. 109 (2016) 573–585 https://doi.org/10.1016/j.cherd.2016.03.002.
[51] Y. Li, Q. Du, T. Liu, X. Peng, J. Wang, J. Sun, Y. Wang, S. Wu, Z. Wang, Y. Xia, L. Xia, Comparative study of methylene blue dye adsorption onto activated carbon, graphene oxide, and carbon nanotubes, Chem. Eng. Res. Des. 91 (2013) 361–368 https://doi.org/10.1016/j.cherd.2012.07.007.
[52] Z. Yang, H. Yan, H. Yang, H. Li, A. Li, R. Cheng, Flocculation performance and mechanism of graphene oxide for removal of various contaminants from water, Water Res 47 (2013) 3037–3046 https://doi.org/10.1016/j.watres.2013.03.027.
[53] A. Gopalakrishnan, R. Krishnan, S. Thangavel, G. Venugopal, S.-.J. Kim, Removal of heavy metal ions from pharma-effluents using graphene-oxide nanosorbents and study of their adsorption kinetics, J. Ind. Eng. Chem. 30 (2015) 14–19 https://doi.org/10.1016/j.jiec.2015.06.005.
[54] Y. Zhang, Y. Cheng, N. Chen, Y. Zhou, B. Li, W. Gu, X. Shi, Y. Xian, Recyclable removal of bisphenol A from aqueous solution by reduced graphene oxide–magnetic nanoparticles: adsorption and desorption, J. Colloid Interface Sci 421 (2014) 85–92 https://doi.org/10.1016/j.jcis.2014.01.022.